HOKKAIDO UNIVERSITY

Title	Nanostructural characterization of ordered gold particle arrays fabricated via aluminum anodizing, sputter coating, and dewetting
Author(s)	Ikeda, Hiroki; Iwai, Mana; Nakajima, Daiki et al.
Citation	Applied surface science, 465, 747-753 https://doi.org/10.1016/j.apsusc.2018.09.229
Issue Date	2019-01-28
Doc URL	https://hdl.handle.net/2115/80361
Rights	©2019. This manuscript version is made available under the CC-BY-NC-ND 4.0 license http://creativecommons.org/licenses/by-nc-nd/4.0/
Rights(URL)	https://creativecommons.org/licenses/by-nc-nd/4.0/
Type	journal article
File Information	Manuscript (Kikuchi).pdf

Hokkaido University Collection of Scholarly and Academic Papers : HUSCAP

Nanostructural Characterization of Ordered Gold Particle Arrays Fabricated via Aluminum Anodizing, Sputter Coating, and Dewetting

Hiroki Ikeda, Mana Iwai, Daiki Nakajima, Tatsuya Kikuchi*, Shungo Natsui, Norihito Sakaguchi, Ryosuke O. Suzuki

Faculty of Engineering, Hokkaido University
N13-W8, Kita-ku, Sapporo, Hokkaido, 060-8628, Japan

*Corresponding author: Tatsuya Kikuchi
TEL: +81-11-706-6340
FAX: +81-11-706-6342
E-mail: kiku@eng.hokudai.ac.jp

Abstract

Gold nanoparticles were fabricated on an ordered aluminum dimple array via aluminum anodizing, sputter coating, and thermal treatment, and the transformation behavior and nanostructural characterization were investigated in detail. Electropolished aluminum specimens were anodized in an oxalic acid solution under self-ordering conditions at 40 V, and then the porous alumina was selectively dissolved to expose an ordered aluminum dimple array with each dimple measuring 100 nm. A thin layer of gold was coated onto the dimple array, and a thermal treatment was subsequently performed. The gold layer was transformed into numerous particles by the thermal treatment due to dewetting. When the values of gold layer thickness, thermal treatment temperature, and thermal treatment duration were optimized, the gold particles were located at the bottom of each aluminum dimple. Consequently, multiply-twinned particles with polygonal and elliptical shapes were regularly distributed on the aluminum dimple array treated at 473 K. Although the rate of the transformation induced by dewetting increased with the temperature of the thermal treatment, non-uniform gold nanostructures were formed by extended thermal treatment at 873 K. The gold particles formed on the aluminum surface exhibited excellent adhesion upon ultrasonication.

Keywords: Aluminum anodizing; Dimple array; Dewetting; Gold nanoparticles; Ordered array

1. Introduction

Anodizing aluminum in a variety of acidic electrolyte solutions under appropriate operating conditions causes the self-ordering of anodic porous alumina (anodic porous oxide films), and consequently, ordered porous alumina with a periodic nanostructure can be obtained on an aluminum substrate [1-3]. The periodicity (interpore distance) and diameter of the nanoscale pores can easily be controlled by choosing the appropriate electrolyte species [4-9], anodizing conditions [10-13], and post-chemical treatment, such as pore widening [14-16]. In addition, a large-scale porous alumina film can be fabricated via self-ordered anodizing combined with nanoimprint lithography [17-19]. Such ordered porous alumina has been widely used in various nanoscale applications such as surface-enhanced Raman scattering (SERS) [20,21], plasmonic devices [22,23], and multi-band light emitters [24].

After the self-ordered anodizing process, the porous alumina is removed from the aluminum substrate by chemical dissolution in a mixture of chromic acid and phosphoric acid, and an ordered aluminum dimple array with a shape matching the bottom shape of the ordered porous alumina is thus exposed to the surface [25,26]. Because the size of each aluminum dimple accurately corresponds to the interpore distance of the porous alumina, various nanoscale dimple arrays can also be obtained via self-ordered anodizing and subsequent chemical dissolution. These ordered dimple arrays have been used as templates for the fabrication of ordered nanostructures, such as nanoscale spherical lens arrays [27] and photonic crystal materials [28].

When ordered aluminum dimple arrays covered with a thin layer of gold are heated, the gold layer transforms into nanoparticles due to dewetting [29,30]. In this unique process, a thin gold layer with nanoscale thickness is deposited on the ordered dimple array by sputter coating, and the gold layer is then transformed into numerous gold nanoparticles positioned at each dimple through a subsequent thermal treatment. Consequently, these gold nanoparticles are uniformly arranged on the ordered aluminum dimple array. However, the details of the transformation behavior of the thin gold layer under various operating conditions have not been reported so far. In addition, the nanostructure of the gold particles fabricated by this dewetting process has not yet been elucidated.

Several methods for the arrangement of metal nanoparticles on various substrates have been reported by many research groups. Ueno et al. worked on the fabrication of gold nanoblocks with small nanogaps on a glass substrate by electron-beam lithography and lift-off techniques for plasmonic field enhancement [31,32]. Fabrication of size-tunable periodic nanoparticle arrays was achieved by Duyne et al. using nanosphere lithography with an appropriate nanosphere [33-35]. Langmuir-Blodgett method for the fabrication of organically passivated metal nanocrystals has been reported by Heath et al [36]. Self-assembly patterns formed upon solvent evaporation were obtained by number of authors [37]. However, a simple technique for fabricating size-controllable ordered nanoparticle arrays with excellent adhesion must be developed by further investigations.

Herein, we report the formation behavior of ordered gold nanoparticle arrays via the transformation of a thin gold layer deposited on an ordered aluminum dimple array under various operating conditions. The effect of the thickness of the gold layer, temperature of the thermal treatment, and the processing time on the transformation

behavior was investigated in detail. Moreover, the nanostructural characterization of the obtained gold particles is discussed. We found unique transformation behaviors of the gold layer on the aluminum dimple array during the thermal treatment process. In addition, we found the appropriate operating conditions for the transformation and arrangement of the gold layer. As a result, ordered gold nanoparticle arrays with excellent adhesion can easily be obtained on the nanostructured aluminum substrate using simple techniques such as anodizing, sputter coating, and thermal treatment.

2. Experimental

High-purity aluminum plates (99.999 wt%, 0.25 to 0.5 mm thick, GoodFellow, UK) were used as starting material. The aluminum specimens were cut into 20 mm × 50 mm samples, and the lower 20 mm × 25 mm region of the surface was subjected to anodizing. The specimens were ultrasonically degreased in ethanol for 10 min at room temperature and then electropolished in a mixture of 78 vol% CH_3COOH and 22 vol% 70%-$HClO_4$ at 280 K and 28 V for 1 min. A large aluminum plate (99.99 wt%, 0.4 mm thick, Nippon Light Metal, Japan) was used as the cathode, and the solution was slowly stirred with a magnetic stirrer during electropolishing.

The electropolished specimens were immersed in a 0.3 M $(COOH)_2$ solution at 290 K and were anodized at a constant voltage of 40 V for 24 h for the fabrication of ordered porous alumina specimens. It is previously reported that the anodizing of aluminum at 40 V in a 0.3 M $(COOH)_2$ solution causes the formation of ordered porous alumina measuring 100 nm in cell diameter due to self-ordering during anodizing [1,38]. A platinum plate (28 mm × 17 mm, 99.95 wt%, 0.1 mm thick, Furuya Metal, Japan) was used as the cathode, and the solution was stirred with a magnetic stirrer during anodizing. After anodizing, the specimens were immersed in a mixture of 0.20 M CrO_3 and 0.51 M H_3PO_4 at 353 K to dissolve the porous alumina, and an ordered aluminum dimple array was exposed to the surface. The ordering behavior of the dimple array was evaluated by fast Fourier transformation (FFT) with the Image-J software package (Wayne Rasband, National Institute of Health, USA).

A thin layer of gold was deposited onto the aluminum dimple array using a DC magnetron sputter coater (Q150TS, Quorum Technologies, UK). A high-purity gold plate (99.99 wt%, 0.1 mm thick, Furuya Metal) was used as the target, and high-purity argon gas (99.9995%) was used for the chamber atmosphere. The average thickness of the gold layer was accurately controlled to 2–10 nm using a quartz crystal microbalance. The gold-coated specimens were placed in an electric furnace (FT-01VAC-50, Full-Tech, Japan) and heated rapidly to 373–873 K within 100 s. The thermal treatment was performed at each operating temperature for up to 24 h in an ambient atmosphere. After the thermal treatment, the electric furnace was cooled to room temperature. The adhesion of the gold nanoparticles formed on the aluminum surface was examined by ultrasonication (55 W, 40 kHz, US-1R, AS-ONE, Japan) in ethanol for up to 30 min.

The surface of the anodized, gold-coated, and thermally treated specimens was examined by field emission scanning electron microscopy (FE-SEM, JSM6500F, JEOL, Japan) and atomic force microscopy (AFM, Nanocute, Hitachi High-Technologies, Japan). The specimens were also examined by spherical aberration-corrected scanning transmission electron microscopy (Cs-corrected STEM, Titan G2 60-300, FEI, USA). For the (S)TEM observation of the horizontal cross-sections, the specimens were pasted

on a single-hole copper grid (Nisshin EM, Japan) with an epoxy resin. The aluminum substrate was thinned from the back by an argon ion beam using a precision ion polishing system (PIPS, Gatan). For the (S)TEM observation of the vertical cross-sections, the specimens were embedded into an epoxy resin (EPON812, TAAB Laboratories Equipment, UK) and then thinned by ultra-thin sectioning using an ultra-microtome (PowerTome X, Boeckeler Instruments, USA) and a diamond knife (NACC 10390SU, Micro Star Technologies, USA).

3. Results and Discussion

An electropolished aluminum specimen was anodized in a 0.3 M oxalic acid solution at 40 V for 24 h to fabricate an ordered porous alumina specimen. Figure 1a shows the SEM image of the aluminum dimple array formed by the subsequent chemical dissolution of the porous alumina in a CrO_3/H_3PO_4 solution. Although a slightly irregular distribution with pentagonal or heptagonal dimples was observed on the surface, an ordered aluminum dimple array with numerous hexagonal dimples was obtained upon long-term anodizing at 40 V. The inset shows the FFT image of the dimple array and exhibits a clear spot pattern based on the ideal dimple arrangement.

Figure 1b and 1c show the three-dimensional AFM image and corresponding vertical cross-section of the ordered dimple array. Each aluminum dimple possesses a hemispherical nanostructure, and six convex regions were formed at the triple points and were surrounded by three adjacent hexagonal dimples. In addition, the edges between each convex region were not flat. Such a nanostructure corresponds to the bottom shape of the ordered porous alumina. The average diameter and depth of the fabricated aluminum dimples were measured to be 100.1 nm and 24.5 nm by SEM and AFM, respectively. After the chemical dissolution of the porous alumina in a CrO_3/H_3PO_4 solution, a thin native oxide film containing trivalent chromium ions and phosphate ions was formed on the aluminum surface in an ambient atmosphere [39]. This ordered aluminum dimple array was used as the starting nanostructured substrate for the fabrication of ordered gold particle arrays.

The aluminum dimple arrays were covered with a thin gold layer measuring 2–10 nm in thickness (δ) by sputter coating and were then heated at T_d = 473–873 K for 1 h. Figure 2a shows the SEM images of the surface of the gold-coated specimens after thermal treatment at 473 K. Although the thin gold layer was transformed into numerous gold nanoparticles on each aluminum dimple array during the thermal treatment, the gold nanostructure greatly differs depending on the thickness of the gold layer. For δ = 2 nm, numerous narrow gold particles measuring several nanometers to 10 nm were distributed at the bottom, edge, and convex regions of the aluminum dimples. For the thinnest gold film, the gold particles were formed on the aluminum dimple arrays (i.e., independently of the dimple array), and an irregular gold particle distribution with various diameters was formed on the surface.

The size of the gold particles formed by thermal treatment increased with the thickness of the gold layer (δ = 6–8 nm), and the gold particles were individually located on the bottom of each aluminum dimple. Although several gold particles were combined with adjacent particles (forming “peanut” particles), an ideal gold particle distribution was obtained by sputter coating a gold layer of thickness δ = 6–8 nm. However, a continuous gold layer consisting of larger gold particles was obtained on the

dimple arrays by excess sputter coating with δ = 10 nm. This non-uniform continuous layer is due to the overflow of the thicker gold film from each aluminum dimple.

Figure 2b shows the SEM images of the surface of the gold-coated specimens after thermal treatment at the higher temperature of 873 K for 1 h. Similar transformation behaviors to those shown in Fig. 2a were observed on each aluminum dimple array, and an ordered gold distribution was obtained by sputter coating with δ = 6 nm. However, in contrast to the behavior at low temperature, many gold particles with different contrasts, such as black, gray, and white hues, were distributed on the surface. In addition, a characteristic undefined nanostructure, similar to that of melted gold particles, was obtained by the formation of a thicker gold layer of δ = 10 nm (yellow arrows). These irregular gold nanostructures formed at high temperature will be discussed later in the section on STEM observations. Henceforth, the thickness of the gold layer formed by sputter coating was fixed to δ = 6 nm.

The time-dependent changes in the transformation behavior of the thin gold layer during thermal treatment were investigated by SEM and STEM, and the corresponding images are shown in Figure 3. The shape of the dimple array was maintained after sputter coating of the gold layer, and an ordered nanostructure similar to that shown in Fig. 1 was formed on the surface (thermal treatment time, t_d = 0). However, the gold layer formed on the aluminum dimple arrays possessed many narrow gaps measuring a few nanometers, and the uncoated aluminum substrate was partially exposed to the surface according to the high-angle annular dark field (HAADF) STEM observation and corresponding EDS measurement (Fig. 3, left). The gold layer formed by sputter coating consisted of numerous nanoscale particles measuring a few nanometers in diameter, as seen in the high-magnification HAADF–STEM image.

The gold-coated aluminum dimple array was heated at 473 K for up to t_d = 24 h for dewetting. Interestingly, the thin gold layer moved to the bottom of the aluminum dimples after 10 min of thermal treatment. In this short thermal treatment, adjacent gold particles were still aggregated, and a continuous gold nanostructure with wide gaps was observed on the aluminum dimple arrays. The gold structure was gradually torn by further thermal treatment for t_d = 15 min and 30 min, and individual gold particles were located on the bottom of aluminum dimples at t_d = 3 h and 24 h. Although several isolated gold particles measuring less than 10 nm in diameter were observed on the edges of the dimple arrays, an ordered gold particle array measuring approximately 63 nm in diameter and 100 nm in periodicity was successfully fabricated by extended thermal treatment at 473 K.

Shi et al. reported that a thin gold film formed by helicon sputtering was transformed into gold islands with varying nanoscale diameters via a high-temperature process [40]. The gold layer formed by sputter coating consisted of numerous nanoscale particles, and these gold particles may transform to a minimum energy state to counter the tension at their surface at high temperature. Therefore, the size of the gold particles increases to decrease the surface-area-to-volume ratio. The thin gold layer was transformed into gold particles on the bottom of ordered dimples, which act as molds. As a result, numerous gold particles were regularly distributed on the aluminum surface. Here, the key parameter in the formation of ordered gold particles was the coating thickness (Fig. 2). An appropriate coating thickness should be selected according to the dimple size and volume; thus, a thickness of 6 nm was chosen for the formation of

ordered gold particles on aluminum dimples measuring 100 nm in diameter, which were fabricated by oxalic acid anodizing at 40 V. Therefore, the thickness of the gold layer should be reduced to fabricate smaller gold particle arrays using a smaller aluminum dimple array formed by sulfuric acid anodizing.

The gold-coated aluminum specimens were heated at various temperatures to investigate the effect of temperature on the transformation behavior of the thin gold layer. Figure 4a shows the SEM images of the surface of the gold-coated specimen after thermal treatment at a relatively low temperature of T_d = 373 K for 1 h and 24 h. Continuous gold layers with narrow gaps, which were similar to the original surface obtained by sputter coating, were observed on each aluminum dimple array, and the nanoscale morphology of the thin gold layer was almost unchanged by extended thermal treatment at 373 K. Therefore, such low-temperature thermal treatment is inappropriate for the transformation of a thin gold layer.

When the temperature of the thermal treatment increased to T_d = 873 K (Fig. 4b), polygonal gold particles were immediately formed on the aluminum dimple array within only one minute; however, the transformation was incomplete and several peanut particles were observed. The shape of the gold particles distributed on the aluminum dimple array changed from polygonal to circular upon further thermal treatment for t_d = 30 min. As seen in the SEM images of the gold particle array at 873 K and 473 K (Fig. 3, t_d = 24 h), the diameter of the gold particles formed at 873 K was smaller than those formed at 473 K, and the particles was quasi circular in shape due to the high-temperature thermal treatment. On the other hand, weak discoloration regions were observed on the aluminum dimple array heated at 873 K for 30 min (yellow arrows). Many such discoloration regions appeared on the surface after further thermal treatment (for example, δ = 6 nm, Fig. 2b). These discoloration regions were investigated by STEM as follows.

Figure 5 shows the low- and high-magnification HAADF–STEM images and the corresponding STEM–EDS elemental distribution maps of aluminum and gold for the gold-coated specimen heated at a high temperature of 873 K for 1 h. Because the HAADF–STEM image exhibits strong atomic number (Z) contrast, the gold distribution on the aluminum surface can be well-understood (light gray hue in the HAADF–STEM image). Although several circular gold particles were formed on each aluminum dimple array, an extremely irregular gold distribution, such as overflow from the dimple, combination with other adjacent particles, and extinction from the dimple, was observed on the aluminum surface. The light gray region shown in the HAADF–STEM image is in good agreement with the gold distribution obtained by the STEM–EDS measurement. Long-term thermal treatment at high temperature for dewetting leads to the formation of such non-uniform gold distributions, which may be due to the excess surface diffusion of the gold particles. Therefore, an accurate control of the operating temperature and time during dewetting is required for the fabrication of ordered gold particle arrays.

Figure 6 shows the HAADF–STEM image and corresponding STEM–EDS elemental distribution maps for the specimen heated at a low temperature of 473 K for 24 h. In contrast to the surface heated at high temperature shown in Fig. 5, ordered gold particles without any defects were distributed on the aluminum dimple arrays. The HAADF–STEM image is in good agreement with the gold distribution obtained by the EDS measurement. The shape of the gold particles was somewhere between circular

and polygonal, and various nanoscale morphologies were observed due to the low-temperature thermal treatment. However, there was almost no irregular gold deposit on the exposed aluminum surface under this operating condition.

Figure 7 shows the bright field (BF) and high-resolution (HR) TEM images of the ordered gold particle array fabricated at 473 K for 24 h. It is clear that the gold particles formed by dewetting possess a polycrystalline structure, and many straight boundaries with different contrasts were observed in the gold particles (yellow arrows). As seen in the HRTEM image of the particle (Fig. 7b), the gold particles possess a round pentagonal morphology with a near five-fold orientation [41,42]. The angles across the boundary in the {111} lattice fringe were measured to be approximately 141° (Fig. 7c). These zigzag boundaries correspond to the typical multiple twinning observed in larger particles [43-45], and the strain of the crystal is relieved by the presence of the twin boundaries [46,47]. Although the number and structure of the multiple twinning depend on each gold particle, similar multiple twinning was observed in other gold particles. Therefore, typical multiply-twinned particles were formed by thermal treatment of the gold-coated aluminum dimple arrays.

Figure 8 shows the BF-TEM image of the vertical cross-section of the ordered gold array formed at 473 K for 24 h. Here, the surface of the dimple array and thermal oxide film is traced with green and blue dotted lines, respectively. A thermal oxide film measuring approximately 8 nm in thickness was formed on the aluminum dimple array by thermal treatment in ambient atmosphere. Polygonal and elliptical gold particles were located on the bottom of each dimple, and the shape of these nanostructures was similar to those in the surface image shown in Fig. 6. From the TEM observations of the horizontal and vertical cross-sections, the gold particles fabricated by dewetting consisted of solid, non-cavity structures.

After the fabrication of the ordered gold particle arrays on the aluminum substrates, the specimens were subjected to ultrasonication for the adhesion test. Figure 9 shows the SEM image of the specimen surface after 30 min of ultrasonication in ethanol at room temperature. A hexagonal gold distribution without any extinction similar to the original arrangement before ultrasonication (Fig. 3) was observed on the aluminum dimple array. Namely, these gold particles, formed via dewetting, exhibited excellent adhesion properties. The fabrication of such metal particle arrays with high adhesion via typical nanoparticle fabrication methods and their subsequent development onto the substrate is difficult; therefore, this method, which is based on the sputter coating and dewetting of a gold layer on an aluminum dimple array, presents a major advantage for the fabrication of ordered particle arrays with excellent adhesion. To achieve an ideal gold distribution over a large area in a short time interval, it may be useful to combine nanoimprinting techniques with anodizing [17].

4. Conclusions

An ordered aluminum dimple array was fabricated by anodizing in an oxalic acid solution at 40 V and the subsequent chemical dissolution of porous alumina. A thin gold layer was formed on the dimple array by sputter coating, and thermal treatment was then carried out for the fabrication of an ordered gold particle array by dewetting. We described in detail the transformation behavior of the thin gold layer during thermal treatment and characterized the nanostructure of the gold particle array. The following

conclusions were drawn from the experimental results of our investigation.
1) The optimal thickness of the gold layer on the ordered aluminum dimple array formed by oxalic acid anodizing at 40 V is approximately 6 nm.
2) The gold layer formed on the aluminum dimple array is gradually transformed into an ordered particle array by thermal treatment at temperatures higher than 473 K. The rate of the transformation induced by dewetting increases with the temperature of the thermal treatment; however, prolonged thermal treatment at the high temperature of 873 K causes irregular gold distribution, such as overflow, combination, and extinction of the gold particles.
3) Multiply-twinned particles with polygonal and elliptical shapes are regularly distributed on the bottom of the aluminum dimples via thermal treatment at 473 K.
4) The ordered gold particle array possesses excellent adhesion properties during ultrasonication.

Acknowledgments

This study was conducted at Hokkaido University and was supported by the "Nanotechnology Platform" Program of the Ministry of Education, Culture, Sports, Science, and Technology (MEXT), Japan. The authors wish to thank Prof. Hiroki Habazaki, Dr. Damian Kowalski, Mr. Keisuke Wada, and Mr. Hikaru Kobayashi for their assistance with the preparation of the TEM specimens, and Mr. Nobuyuki Miyazaki, Mr. Takashi Endo, and Mr. Ryo Oota for their assistance with the SEM and STEM observations. This study was financially supported by the Murata Science Foundation and the Amada Foundation, Japan.

References

1) H. Masuda, K. Fukuda, Ordered metal nanohole arrays made by a two-step replication of honeycomb structures of anodic alumina, Science 268 (1995) 1466-1468.
2) W. Lee, D. J. Park, Porous anodic aluminum oxide: anodization and templated synthesis of functional nanostructures, Chem. Rev., 114 (2014) 7487-7556.
3) G.D. Sulka, Highly ordered anodic porous alumina formation by self-organized anodizing, in: A. Eftrkhari (Ed.), Nanostructured materials in electrochemistry, Wiley-VCH Verlag GmbH & Co. KGaA, Weinheim, 2008, pp. 1-116.
4) A.P. Li, F. Müller, A. Birner, K. Nielsch, U. Gösele, Hexagonal pore arrays with a 50–420 nm interpore distance formed by self-organization in anodic alumina, J. Appl. Phys. 84 (1998) 6023-6026.
5) H. Masuda, K. Yada, A. Osaka, Self-ordering of cell configuration of anodic porous alumina with large-size pores in phosphoric acid solution, Jpn. J. Appl. Phys. 37 (1998) L1340.
6) T. Kikuchi, O. Nishinaga, S. Natsui, R.O. Suzuki, Self-ordering behavior of anodic porous alumina via selenic acid anodizing, Electrochim. Acta 137 (2014) 728-735.
7) T. Kikuchi, O. Nishinaga, S. Natsui, R.O. Suzuki, Fabrication of self-ordered porous alumina via etidronic acid anodizing and structural color generation from submicrometer-scale dimple array, Electrochim. Acta 156 (2015) 235-243.
8) A. Takenaga, T. Kikuchi, S. Natsui, R.O. Suzuki, Exploration for the Self-ordering of Porous Alumina Fabricated via Anodizing in Etidronic Acid, Electrochim. Acta

211 (2016) 515-523.
9) S. Akiya, T. Kikuchi, S. Natsui, N. Sakaguchi, R.O. Suzuki, Self-ordered porous alumina fabricated via phosphonic acid anodizing, Electrochim. Acta 190 (2016) 471-479.
10) L. Zaraska, W.J. Stępniowski, G.D. Sulka, E. Ciepiela, M. Jaskuła, Analysis of nanopore arrangement and structural features of anodic alumina layers formed by two-step anodizing in oxalic acid using the dedicated executable software, Appl. Phys. A 114 (2014) 571-577.
11) W.J. Stępniowski, A. Nowak-Stępniowska, M. Michalska-Domańska, M. Norek, T. Czujko, Z. Bojar, Fabrication and geometric characterization of highly-ordered hexagonally arranged arrays of nanoporous anodic alumina, Pol. J. Chem. Tech. 16 (2014) 63-69.
12) M. Norek, M. Dopierała, W.J. Stępniowski, Ethanol influence on arrangement and geometrical parameters of aluminum concaves prepared in a modified hard anodization for fabrication of highly ordered nanoporous alumina, J. Electroanal. Chem. 750 (2015) 79-88.
13) S. Akiya, T. Kikuchi, S. Natsui, R.O. Suzuki, Optimum exploration for the self-ordering of anodic porous alumina formed via selenic acid anodizing, J. Electrochem. Soc. 162 (2015) E244-E250.
14) L. Zaraska, G.D. Sulka, M. Jaskuła, Anodic alumina membranes with defined pore diameters and thicknesses obtained by adjusting the anodizing duration and pore opening/widening time, J. Solid State Electrochem. 15 (2011) 2427-2436.
15) J. Zhang, J.E. Kielbasa, D.L. Carroll, Controllable fabrication of porous alumina templates for nanostructures synthesis, Mater. Phys. Chem. 122 (2010) 295-300.
16) M. Nagayama, K. Tamura, H. Takahashi, Mechanism of open-circuit dissolution of porous oxide films on aluminium in acid solutions, Corr. Sci. 12 (1972) 133-136.
17) H. Asoh, K. Nishio, M. Nakao, T. Tamamura, H. Masuda, Conditions for fabrication of ideally ordered anodic porous alumina using pretextured Al, J. Electrochem. Soc. 148 (2001) B152-B156.
18) W. Lee, R. Ji, U. Gösele, K. Nielsch, Fast fabrication of long-range ordered porous alumina membranes by hard anodization, Nat. Mater. 5 (2006) 741-747.
19) T.S. Kustandi, W.W. Loh, H. Gao, H.Y. Low, Wafer-scale near-perfect ordered porous alumina on substrates by step and flash imprint lithography, ACS Nano 4 (2010) 2561-2568.
20) T. Kondo, F. Matsumoto, K. Nishio, H. Masuda, Surface-enhanced Raman scattering on ordered gold nanodot arrays prepared from anodic porous alumina mask, Chem. Lett. 37 (2008) 466-467.
21) T. Kondo, H. Masuda, K. Nishio, SERS in ordered array of geometrically controlled nanodots obtained using anodic porous alumina, J. Phys. Chem. C 117 (2012) 244-250.
22) L. Wen, R. Xu, Y. Mi, Y. Lei, Multiple nanostructures based on anodized aluminum oxide templates, Nat. Nanotechnol. 12 (2017) 244-250.
23) T. Ozel, G.R. Bourret, C.A. Mirkin, Coaxial Lithography, Nat. Nanotechnol. 10 (2015) 319-324.
24) M. Norek, M. Michalska-Domańska, W.J. Stępniowski, I. Ayala, A. Bombalska, B. Budner, Multi-band emission in a wide wavelength range from tin oxide/Au

nanocomposites grown on porous anodic alumina substrate (AAO), Appl. Surf. Sci. 287 (2013) 143-149.
25) S. Ono, M. Saito, H. Asoh, Self-ordering of anodic porous alumina formed in organic acid electrolytes, Electrochim. Acta 51 (2005) 827-833.
26) T. Kikuchi, O. Nishinaga, S. Natsui, R.O. Suzuki, Polymer nanoimprinting using an anodized aluminum mold for structural coloration, Appl. Surf. Sci. 341 (2015) 19-27.
27) K. Kawahara, T. Kikuchi, S. Natsui, R.O. Suzuki, Fabrication of ordered submicrometer-scale convex lens array via nanoimprint lithography using an anodized aluminum mold, Microelectron. Eng. 185 (2018) 61-68.
28) C.Y. Peng, C.W. Hsu, C.W. Li, P.L. Wang, C.C. Jeng, C.C. Chang, G.J. Wang, Flexible Photonic Crystal Material for Multiple Anticounterfeiting Applications, ACS Appl. Mater. Interfaces 10 (2018) 9858-9864.
29) X. Fan, Q. Hao, R. Jin, H. Huang, Z. Luo, X. Yang, Y. Chen, X. Han, M. Sun, Q. Jing, Z. Dong, T. Qiu, Assembly of gold nanoparticles into aluminum nanobowl array, Sci. Rep. 7 (2017) 2322.
30) T. Kikuchi, D. Nakajima, H. Ikeda, R. Kondo, K. Kawahara, K. Kunimoto, M. Iwai, Y. Suzuki, S. Akiya, A. Takenaga, O. Nishinaga, S. Natsui, R.O. Suzuki, Advanced functional aluminum materials based on nanostructured surface, J. Jpn. Inst. Light Metals 68 (2018) 211-218.
31) K. Ueno, S. Juodkazis, T. Shibuya, Y. Yokota, V. Mizeikis, K. Sasaki, H. Misawa, Nanoparticle plasmon-assisted two-photon polymerization induced by incoherent excitation source, J. Am. Chem. Soc. 130 (2008) 6928-6929.
32) K. Ueno, S. Juodkazis, V. Mizeikis, K. Sasaki, H. Misawa, Spectrally-resolved atomic-scale length variations of gold nanorods, J. Am. Chem. Soc. 128 (2006) 14226-14227.
33) C.L. Haynes, R.P. Van Duyne, Nanosphere lithography: a versatile nanofabrication tool for studies of size-dependent nanoparticle optics, J. Phys. Chem. B 105 (2001) 5599-5611.
34) T.R. Jensen, M.D. Malinsky, C.L. Haynes, R.P. Van Duyne, Nanosphere lithography: tunable localized surface plasmon resonance spectra of silver nanoparticles, J. Phys. Chem. B 104 (2000) 10549-10556.
35) J.C. Hulteen, D.A. Treichel, M.T. Smith, M.L. Duval, T.R. Jensen, R.P. Van Duyne, Nanosphere lithography: size-tunable silver nanoparticle and surface cluster arrays, J. Phys. Chem. B 103 (1999) 3854-3863.
36) J.R. Heath, C.M. Knobler, D.V. Leff, Pressure/temperature phase diagrams and superlattices of organically functionalized metal nanocrystal monolayers: the influence of particle size, size distribution, and surface passivant, J. Phys. Chem. B 101 (1997) 189-197.
37) T.K. Sau, C.J. Murphy, Self-assembly patterns formed upon solvent evaporation of aqueous cetyltrimethylammonium bromide-coated gold nanoparticles of various shapes, Langmuir 21 (2005) 2923-2929.
38) T. Kikuchi, D. Nakajima, O. Nishinaga, S. Natsui, R.O. Suzuki, Porous Aluminum Oxide Formed by Anodizing in Various Electrolyte Species, Curr. Nanosci. 11 (2015) 560-571.
39) H. Takahashi, M. Nagayama, Surface films formed on aluminum by different pretreatments I. XPS analysis of thickness and chemical composition, J. Surf. Finish.

Soc. Jpn. 36 (1985) 96-103.
40) X. Shi, K. Ueno, N. Takabayashi, H. Misawa, Plasmon-enhanced photocurrent generation and water oxidation with a gold nanoisland-loaded titanium dioxide photoelectrode, J. Phys. Chem. C 117 (2012) 2494-2499.
41) S. Liu, Q. Zhang, Y. Li, M. Han, L. Gu, C. Nan, J. Bao, Z. Dai, Five-fold twinned Pd_2NiAg nanocrystals with increased surface Ni site availability to improve oxygen reduction activity, J. Am. Chem. Soc. 137 (2015) 2820-2823.
42) A.M. Goswami, S. Ghosh, Biological synthesis of colloidal gold nanoprisms using Penicillium citrinum MTCC9999, J. Biomater. Nanobiotech. 4 (2013) 20-27.
43) L.D. Marks, A. Howie, Multiply-twinned particles in silver catalysts, Nature 282 (1979) 196-198.
44) J. Sopoušek, J. Pinkas, P. Brož, J. Buršík, V. Vykoukal, D. Škoda, A. Stýskalík, O. Zobač, J. Vřešťál, A. Hrdlička, J. Šimbera, Ag-Cu colloid synthesis: bimetallic nanoparticle characterisation and thermal treatment, J. Nanomater. 2014 (2014) 638964.
45) S.M. Rupich, E.V. Shevchenko, M.I. Bodnarchuk, B. Lee, D. Talapin, Size-dependent multiple twinning in nanocrystal superlattices, J. Am. Chem. Soc. 132 (2009) 289-296.
46) M.J. Yacamán, J.A. Ascencio, H.B. Liu, J. Gardea-Torresdey, Structure shape and stability of nanometric sized particles, J. Vac. Sci. Technol. B 19 (2001) 1091-1103.
47) C.L. Johnson, E. Snoeck, M. Ezcurdia, B. Rodríguez-González, I. Pastoriza-Santos, L.M. Liz-Marzán, M.J. Hÿtch, Effects of elastic anisotropy on strain distributions in decahedral gold nanoparticles, Nat. Mater. 7 (2008) 120-124.

Figure Captions

Figure 1 a) SEM, b) three-dimensional AFM, and c) cross-sectional AFM images of the ordered aluminum dimple array formed by anodizing in a 0.3 M oxalic acid solution at 290 K and 40 V for 24 h.

Figure 2 SEM images of the gold particle array formed on the aluminum dimple array by thermal treatment at a) 473 K and b) 873 K for 1 h. The average thickness of the gold layer deposited by sputter coating was adjusted to 2–10 nm using a quartz crystal microbalance.

Figure 3 SEM, HAADF–STEM, and corresponding STEM–EDS elemental distribution images of the gold nanostructure during thermal treatment at 473 K for up to 24 h. Henceforth, the thickness of the gold layer deposited by sputter coating was set to 6 nm.

Figure 4 SEM images of the gold nanostructure during thermal treatment at a) 373 K and b) 873 K for different operating times.

Figure 5 HAADF–STEM images and corresponding STEM–EDS aluminum and gold elemental distribution maps of the nanostructure fabricated by thermal treatment at 873 K for 1 h.

Figure 6 HAADF–STEM images and corresponding STEM–EDS aluminum and gold elemental maps of the ordered particle array fabricated by thermal treatment at 473 K for 24 h.

Figure 7 High-resolution BF-TEM images of the ordered gold particle array fabricated by thermal treatment at 473 K for 24 h.

Figure 8 BF-TEM image of the vertical cross-section of the ordered gold particle array fabricated by thermal treatment at 473 K for 24 h.

Figure 9 SEM image of the ordered gold particle array formed on the aluminum dimple array after ultrasonication in ethanol for 30 min.

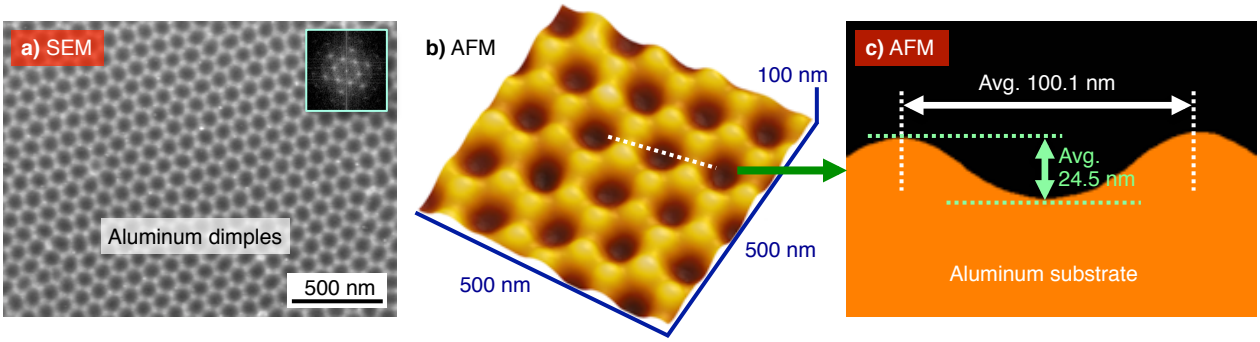

a) SEM
Aluminum dimples
500 nm
b) AFM
100 nm
500 nm
500 nm
c) AFM
Avg. 100.1 nm
Avg.
24.5 nm
Aluminum substrate

Figure 1.

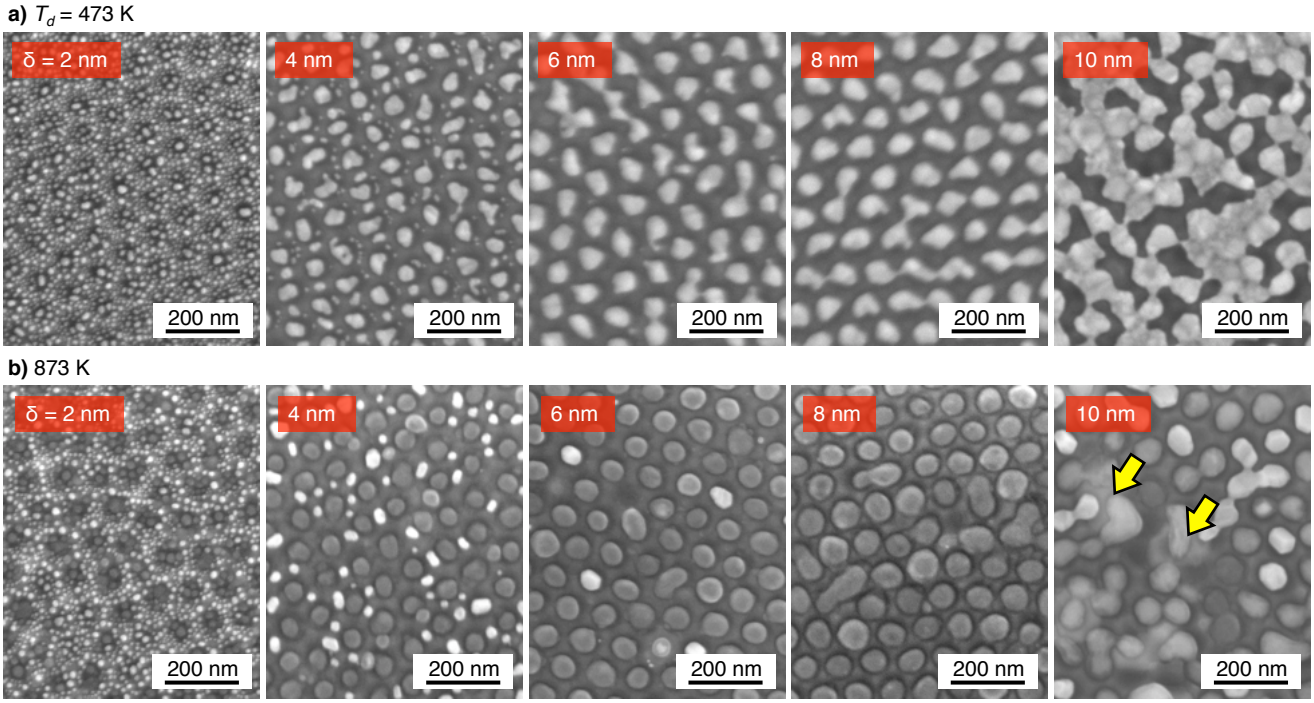


Figure 2.

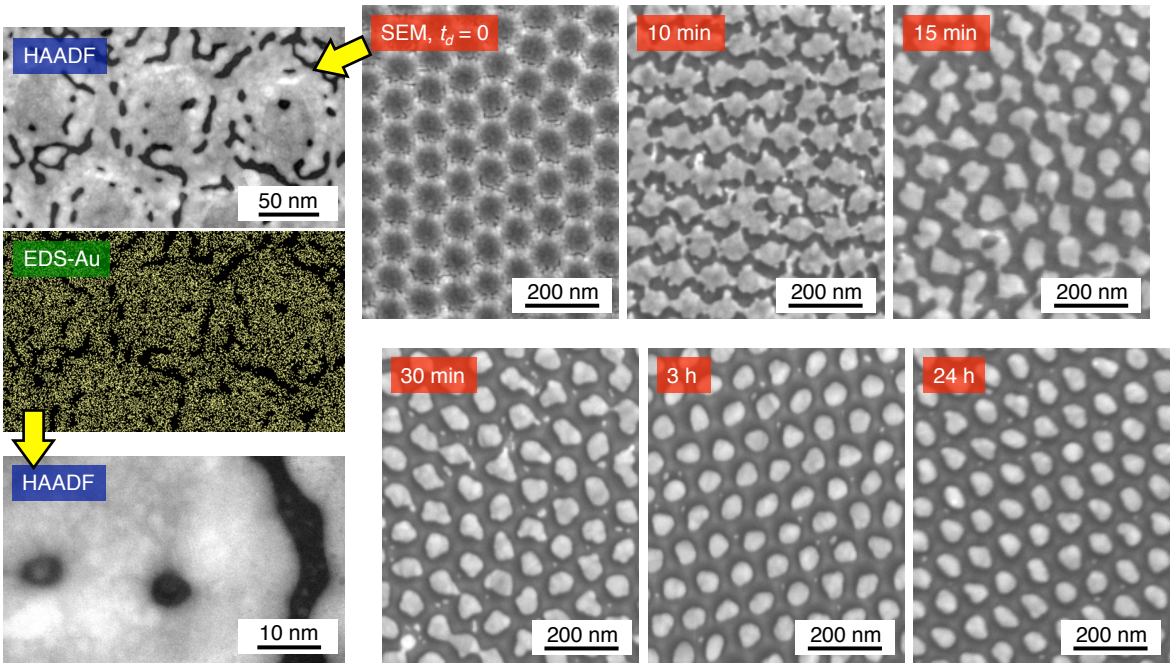

HAADF
50 nm
EDS-Au
HAADF
10 nm
SEM, $t_d = 0$
200 nm
10 min
200 nm
15 min
200 nm
30 min
200 nm
3 h
200 nm
24 h
200 nm

Figure 3.

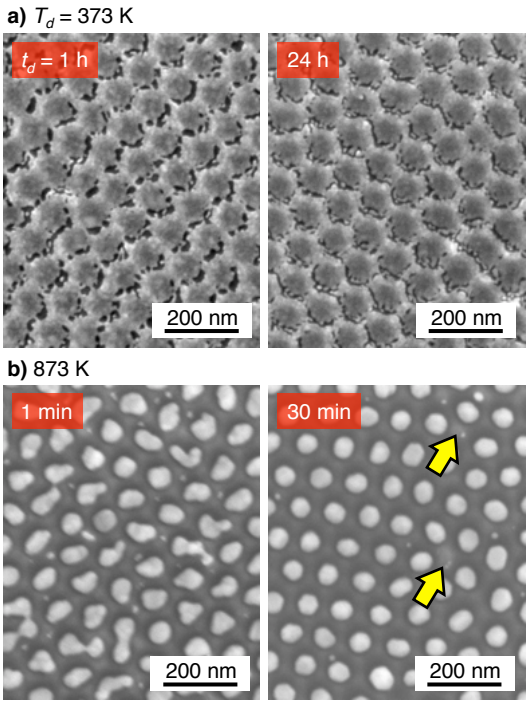


Figure 4.

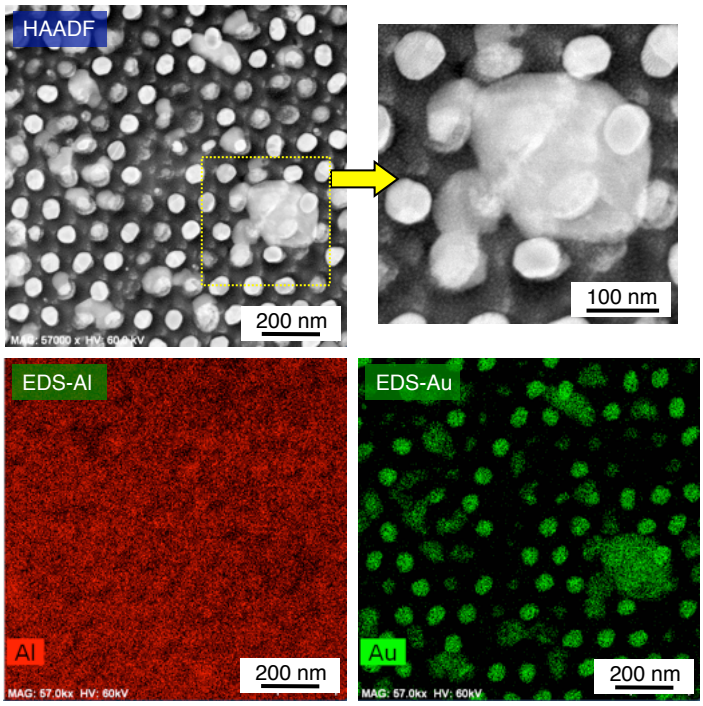


Figure 5.

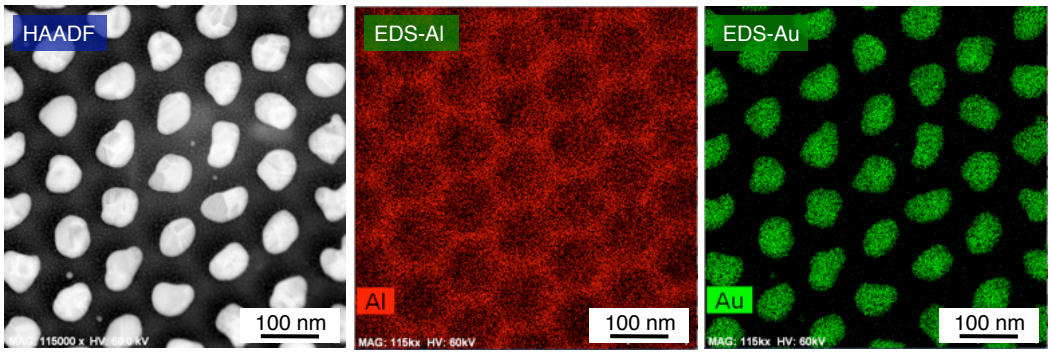

HAADF
100 nm
EDS-Al
Al
100 nm
MAG: 115kx HV: 60kV
EDS-Au
Au
100 nm
MAG: 115kx HV: 60kV

Figure 6.

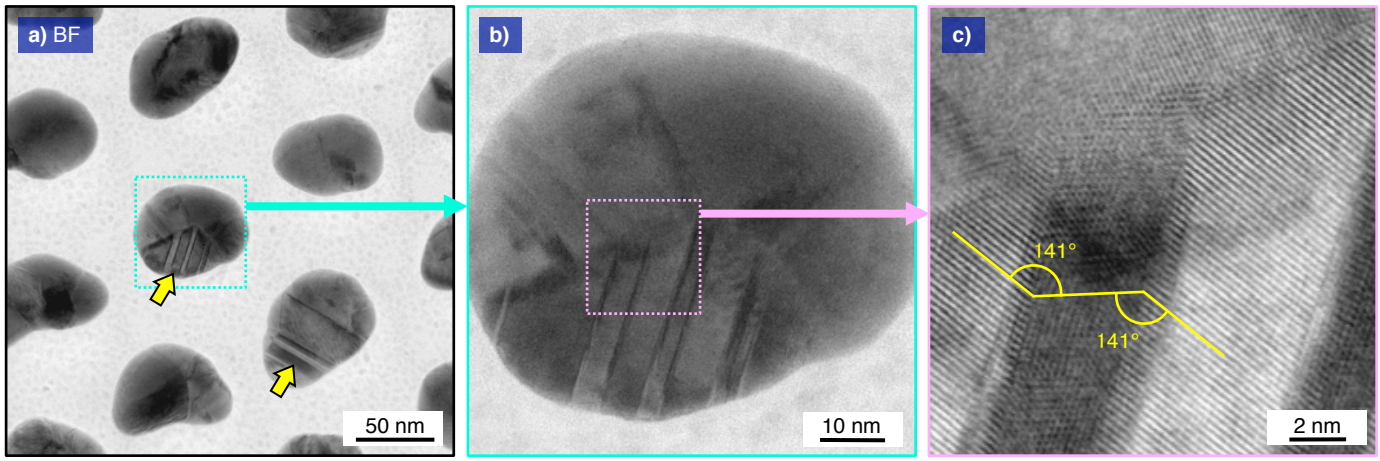


Figure 7.

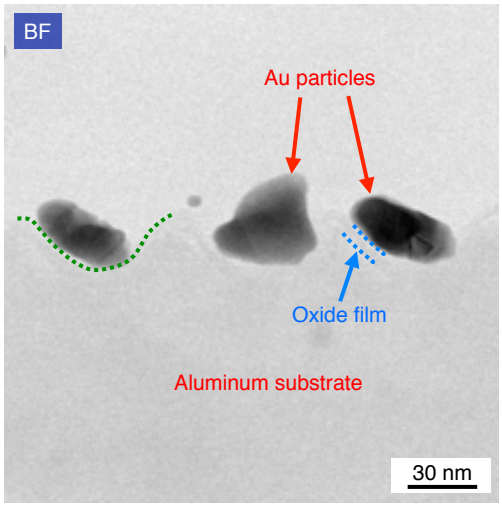


Figure 8.

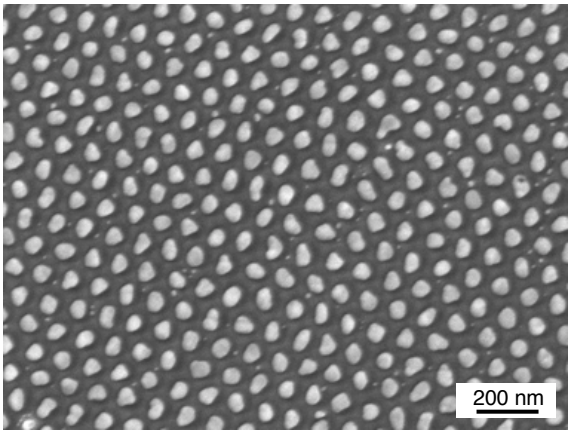


Figure 9.